

Imaging Intracellular pH in Live Cells with a Genetically-Encoded Red Fluorescent Protein Sensor

Mathew Tantama, Yin Pun Hung, Gary Yellen

Department of Neurobiology, Harvard Medical School, Boston, Massachusetts, 02115.

*gary_yellen@hms.harvard.edu.

Available Supporting Information Contains:

Methods

Supplemental Figure S1-S6 and Discussion

Supplemental Table S1

Supplemental References

Materials and Methods. Chemicals were purchased from Sigma-Aldrich unless otherwise noted. Cell culture media and supplements were purchased from Invitrogen unless otherwise noted. Error bars are standard errors.

Development of pHRed.

In the development of mKeima, an early-stage precursor exhibited two pH-dependent fluorescence excitation peaks at 452 and 580 nm, and the 452 nm peak was attenuated with four mutations: S61F, I92T, F158Y and S213A.¹ Of these mutations, the side chains of residues 92 and 158 are exterior facing, and residues 61 and 92 were further mutagenized in subsequent stages of development. Residue 158 is adjacent to D157, a residue important for ESPT;^{2,3} however, the F158Y mutation is sterically conservative. In contrast, the side chain of residue 213 projects towards the chromophore,^{2,3} and therefore we rationalized that reversing the S213A mutation would be a good starting point for recovering the 452 nm peak. Indeed, the mKeima-A213S mutant exhibits dual excitation peaks that respond ratiometrically to pH (Figure 1a). Because of proximity to the chromophore, we also conducted random mutagenesis of residues 60 and 61, but no improved variants were identified.

As for mKeima, the “reverse” pH dependence³ of pHRed’s fluorescence response is reminiscent of the behavior of the GFP-derived pHluorins,⁴ and it is opposite the trend observed for *avGFP*.⁵ In mKeima the reverse pH dependence is a result of chromophore interactions with S142 and D157.³ The carboxylate of D157 stabilizes the protonated chromophore in a *trans* conformation, but under acidic conditions in which D157 is protonated, hydrogen bonding with S142 stabilizes the anionic chromophore in a *cis* conformation.³ However, at alkaline pH D157 may also stabilize the *cis*-protonated chromophore, and the role of the isomerization is not clear.² Furthermore, residues S142 and D157 also provide a proton transfer network for ESPT following excitation of the protonated chromophore, and excitation of either ionization state results in red fluorescence emission.

A synthetic gene encoding mKeima (Genscript) was subcloned into the pRSetB (Invitrogen) bacterial expression vector, appending a 7xHis tag. Mutations were introduced by site-directed mutagenesis or by degenerate oligonucleotides and overlap PCR. Mutants were transformed into DH5 α *E. coli* and grown in 96-well deep-well plates in 1.5 mL of YT media overnight at 37°C with shaking followed by room temperature shaking for 1 to 3 days. Bacterial pellets were collected by centrifugation, triturated in lysis buffer (1X CellLyticB, 100 mM MOPS, 50 mM KCl, 5

mM NaCl, 0.5 mM MgCl₂, pH 7.4 KOH), transferred to HisSelect Nickel-Affinity 96-well plates (Sigma), and incubated overnight at room temperature with shaking to capture protein. Capture plates were then washed three times with tris-buffered saline with 0.1% Triton-X100 and three times with MOPS wash buffer (Lysis buffer excluding CellLyticB). Plates were then incubated at room temperature with shaking for 4 to 6 hours in elution buffer (wash buffer plus 20 mM imidazole and 0.1% BSA). Clear bottom black 96-well plates (Nunc) were pre-blocked with elution buffer. Fluorescence of mutant proteins was screened using a Synergy 4 fluorescence plate reader (BioTek).

Initial Expression and Purification. pHRed containing an N-terminal 7xHis tag was expressed in DH5 α cells as described above except scaled to a 10 to 30 mL culture volume. Protein was purified using the Qiagen NiNTA Quick Spin Columns according to manufacturer instructions. Eluate was dialyzed into storage buffer (10 mM HEPES, 120 mM KCl, 10 mM NaCl, 0.5 mM MgCl₂, 20% glycerol, pH 7.4 KOH) with two buffer changes at 4°C, stored at -20°C to 4°C for use within 5 days or stored at -80°C for later use.

Initial Characterization of Purified pHRed in Solution. For pH titrations buffer contained 10 mM of acetate, MES, MOPS, Bicine, and CHES and 100 mM of NaCl (pH with NaOH) or KCl (pH with KOH) or K-Gluconate (pH with KOH). Protein samples were diluted 20 to 40 fold to ~2 μ M, and fluorescence was measured in a fluorescence plate reader or in a cuvette spectrofluorometer for more detailed spectra (Fluoromax, Horiba Jobin Yvon). To test for interferences, consecutive additions of MgCl₂, CaCl₂, H₂O₂, and DTT were made to samples diluted into NaCl, KCl, or K-gluconate buffers. For temperature dependence, samples were measured in sealed plates to prevent evaporation. Fluorescence was measured at room temperature (21°C) first. Temperature was then consecutively increased to 25°C, 31°C, and 37°C, and the samples and instrument were allowed to equilibrate before measuring fluorescence. For sensitivity to bicarbonate, solutions were titrated with NaHCO₃ from pH 4.9 to 8.2. Protein was diluted into bicarbonate buffers and fluorescence measured within 5 minutes of pH measurement to minimized pH variations in the absence of a controlled CO₂ atmosphere. For filter based plate reader measurements, 440/20 nm and 575/15 nm excitation and a 635/32 nm emission filters were used.

Expression in Neuro2A Cells. pHRed was subcloned into the GW1 (British Biotech) mammalian expression vector. DNA was prepared from DH5 α cells using Qiagen High Speed MaxiPrep

kits. Neuro2A (ATCC CCL-131) cells were cultured at 37°C in 5% CO₂ humidified air atmosphere in MEM media containing 10% bovine calf serum (Invitrogen) and passed every 3 to 4 days. For expression, cells were plated onto protamine coated 18 mm diameter, #1.5 glass coverslips (Thermo). Four to six hours later, cells were transfected using Effectene (Qiagen) according to manufacturer's instructions. The following day media was changed to low glucose DMEM containing 1% bovine calf serum and 10 μ M all *trans*-retinoic acid to induced neurite extension. Cells were imaged 24 to 72 hours after media change.

Cell Treatments and Nigericin pH Calibrations. Cells were imaged in continuously flowing (2 mL/min) artificial cerebrospinal fluid (ACSF in mM: 130 NaCl, 4 KCl, 2 CaCl₂, 1 MgCl₂, 20 sucrose) buffered with 25 mM HEPES, pH 7.4 (NaOH) except for Figure 3 where ACSF was buffered with 25 mM NaHCO₃ bubbled with 5% CO₂/95% air. ACSF was warmed to 34 \pm 1°C with an inline heater placed just before the perfusion chamber except for FLIM experiments conducted at room temperature. Glucose was added to concentrations indicated in the text and osmotic balance was maintained with sucrose (~325 mOsmol to match complete DMEM culture media). For nigericin experiments, NaCl was replaced with KCl, and 2-5 μ M nigericin was used.

Intensity Ratio Imaging. Cells were imaged on a Nikon Eclipse TE300 inverted microscope mounted with an Andor Revolution Differential Spinning Disk (DSD) unit for optical sectioning controlled by iQ software. Excitation light from a Prior Lumen Pro was passed through 445/20 nm, 482/18 nm, or 578/16 nm Semrock filters. The DSD unit contained a Chroma 59022bs dichroic, Semrock 492 nm short pass, Omega 490 nm short pass, and Omega 590 nm short pass filters. Excitation light was passed through Semrock 525/39 nm or 629/56 nm filters. In a typical experiment, images were taken in succession at 10 second intervals with 2x2 binning and 200 to 400 ms exposure times using a Nikon Plan Apo VC 20X/0.75NA dry objective. Background and bleed-through of Perceval fluorescence into the pHRed channel were subtracted before ratios were calculated. There is a minimal amount of bleedthrough (5%) of Perceval green fluorescence into the pHRed red channel when excited at the shared wavelength of 445 nm. Pixel-by-pixel ratios were calculated, regions of interest were drawn around cells, and average measurements were calculated with thresholding using ImageJ software.

Perceval is a dual excitation ratiometric sensor that responds to changes in the ATP:ADP ratio.⁶ The F_{485}/F_{445} fluorescence intensity ratio (R) increases in response to increasing ATP:ADP with a half maximal response at ATP:ADP ~ 0.5. The occupancy of the sensor is calculated as $(R - R_{\min}) / (R_{\max} - R_{\min})$. R_{\min} and R_{\max} are estimated at the end of *each* experiment in 0 or 25 mM glucose, respectively, and the ratios are pH-corrected as described below.

Two-Photon FLIM. Protein samples and cells were imaged on an upright microscope with a 10X dry objective modified for lifetime imaging built in house by G.Y. and Bernardo Sabatini. Samples were excited using a tunable Ti:Sapphire 80 MHz laser (Coherent, Chameleon Vision II), and a time-correlated single-photon counting board (Becker and Hickl SP-830) was used to measure fluorescence decays. Fluorescence emission was collected by a photomultiplier tube (Hamamatsu 47422) through a 700 nm long pass and 630/60 nm filters. Data was collected and analyzed using Matlab software provided by Ryohei Yasuda and Bernardo Sabatini and modified by G.Y. The empirical mean lifetimes were measured by averaging over a 9 ns window. The zero time offset for the averaging window was estimated to be the time of peak intensity as determined by fitting the fluorescence

decays to a bi-exponential function convoluted with a Gaussian instrument response function. There was no difference in estimated zero time offsets using either a Gaussian instrument response function or an experimental response function. The fitting approach provides a robust automated method for determining the zero time offset and averaging window. The fitted lifetimes themselves were not used because the empirical mean lifetimes provide a fitting-independent measurement. These empirical mean lifetimes are plotted in Figures 2b and 2c.

Note that the pH changes in Figure 1f and Figure 2b differ in kinetics. This is an artifact of the different perfusion systems attached to the ratio imaging and FLIM instruments. Thus the difference in the rate of the pH-dependent ratio and lifetime changes reflects differences in solution exchange, not any fundamental photophysical peculiarity.

Spectroscopy for Extinction Coefficient and Quantum Yield Determinations. For spectroscopy, pHRed and mKeima proteins were expressed and purified as described above. However, proteins were dialyzed into a low buffering strength solution (5 mM MOPS, pH 7.3, 300 mM NaCl, 10% glycerol). For pH studies, the solutions contained 300 mM NaCl and 50 mM of one of the following buffers: MES, pH 5.5; MES, pH 6.0; MOPS, pH 6.5; MOPS, pH 7.0; MOPS, pH 8.0; Bicine, pH 8.5; Bicine, pH 9.0; CHES, pH 10.0.

The concentration of protein containing mature chromophore was measured in 1M NaOH. mKeima and pHRed have the same QYG-derived chromophore as DsRed. Alkaline denaturation of the protein exposes the chromophore, and hydrolysis of the chromophore acylimine produces a GFP-like chromophore. In agreement, both mKeima and pHRed exhibit 446 nm peak absorbance in 1M NaOH. The extinction coefficient of this chromophore measured for DsRed in 1M NaOH was close to that for GFP ($\epsilon_{446} = 4 \times 10^4 \text{ M}^{-1} \cdot \text{cm}^{-1}$).⁷ Therefore absorbance at 446 nm in 1M NaOH can be used to measure the concentration of mature chromophore.⁸ Mature protein concentrations were measured at several dilution on several days, and protein concentrations were consistent. For direct comparison with literature values, total protein concentration of mKeima was determined by colorimetric bicinchoninic acid (BCA) assay. Comparison of the two methods indicate that ~60% of the mKeima protein contains mature chromophore, consistent with previously published reports.² Furthermore, the extinction coefficient determined using BCA-assayed total protein concentration values is $\sim 15000 \text{ M}^{-1} \cdot \text{cm}^{-1}$ at pH 7.5, very consistent with other published reports where the extinction coefficient was also determined with respect to BCA-assayed total protein concentration.^{1,9} In order to provide an accurate description of the mature mKeima and pHRed we henceforth used the protein concentration determined by the alkaline denaturation method as others have.^{8,10}

For pH-dependent extinction coefficient measurements, proteins were diluted in appropriate buffers at 3 or 4 different concentrations (~5-20 μ M), and the extinction coefficients were calculated according to the Beer-Lambert equation.

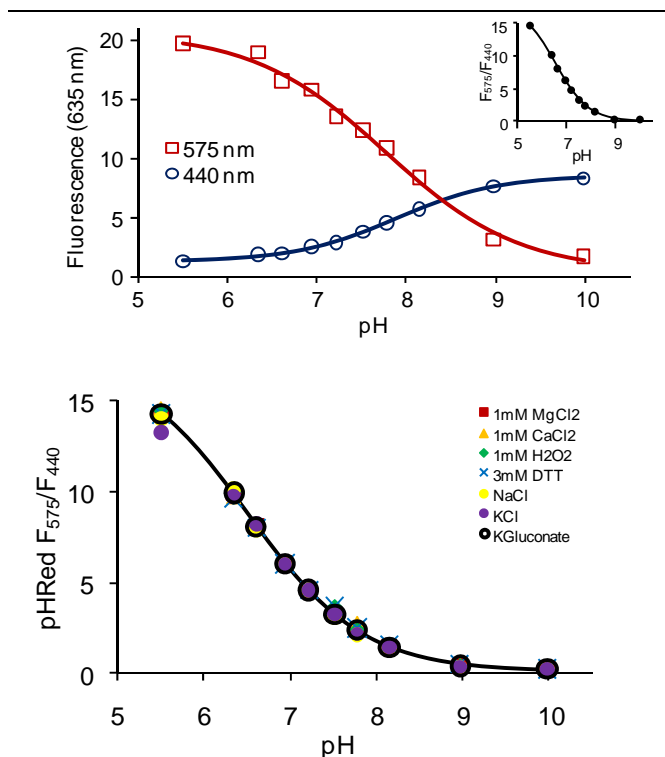
For pH-dependent quantum yields, proteins were diluted in appropriate buffers to absorbances of 0.001 to 0.01, and the fluorescence vs. absorbance slopes were measured through 7 to 9 data points. For 440 nm excitation, mKeima at pH 7.5 was used as the reference standard (QY = 0.24).¹ For 585 nm excitation, sulforhodamine 101 in ethanol was used as the reference standard with correction for the difference in refractive index (QY = 0.95).¹¹

Supplemental Figures, Tables, and Discussions.

pHRed's Fluorescence Intensity and Intensity Ratio (Related to Figure 1a-c) The maximal fluorescence intensity change with 575 nm excitation is of a larger magnitude than the maximal fluorescence intensity change with 440 nm excitation (Supplemental Figure S1). As a result the intensity ratio pH response is acid shifted. While both F_{575} and F_{440} respond to pH with a $pK_a \sim 7.8$, the F_{575}/F_{440} ratio responds with a $pK_a \sim 6.6$.

The same is true for mKeima fluorescence intensities, but for mKeima the fluorescence intensities respond to pH with a $pK_a \sim 6.6$. This causes the intensity ratio of mKeima to respond to pH with a $pK_a < 6$, a major reason why pHRed is better suited for monitoring intracellular pH compared to mKeima.

pH Response is Insensitive to Various Factors (Related to Figure 1a-c). The pH-dependent fluorescence of pHRed was insensitive to differences in buffer ion composition (Mg^{2+} , Ca^{2+} , K^+ , Na^+ , Cl^- , HCO_3^-), oxidative stress (H_2O_2 , dithiothreitol), and temperature ($pK_a(21^\circ C)=6.6$; $pK_a(25^\circ C)=6.7$; $pK_a(31^\circ C)=6.7$; $pK_a(37^\circ C)=6.7$), so there should be minimal artifacts due to these factors (Supplemental Figure S1).

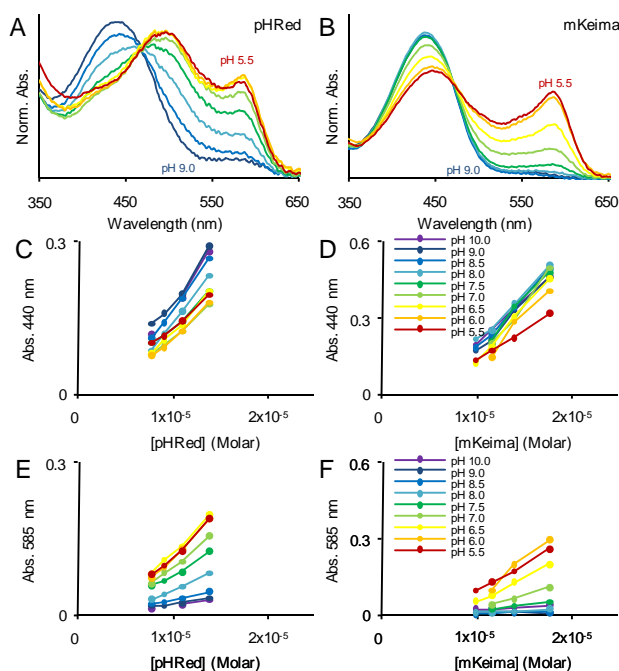


Supplemental Figure S1. Top: Scaled pH responses of pHRed fluorescence intensities. F_{575} and F_{440} both exhibit a pK_a of ~ 7.8 , but F_{575} changes nearly 2-fold more in magnitude than F_{440} , causing the ratio to reach half-maximal response at a lower pK_a of 6.6 (inset). Bottom: The pH response of pHRed's F_{575}/F_{440} intensity ratio was not significantly affected by changes in buffer concentrations of Mg^{2+} , Ca^{2+} , Na^+ , K^+ , Cl^- , HCO_3^- , gluconate $^-$, hydrogen peroxide, or dithiothreitol (symbols overlay one another closely on the fitted solid black curve).

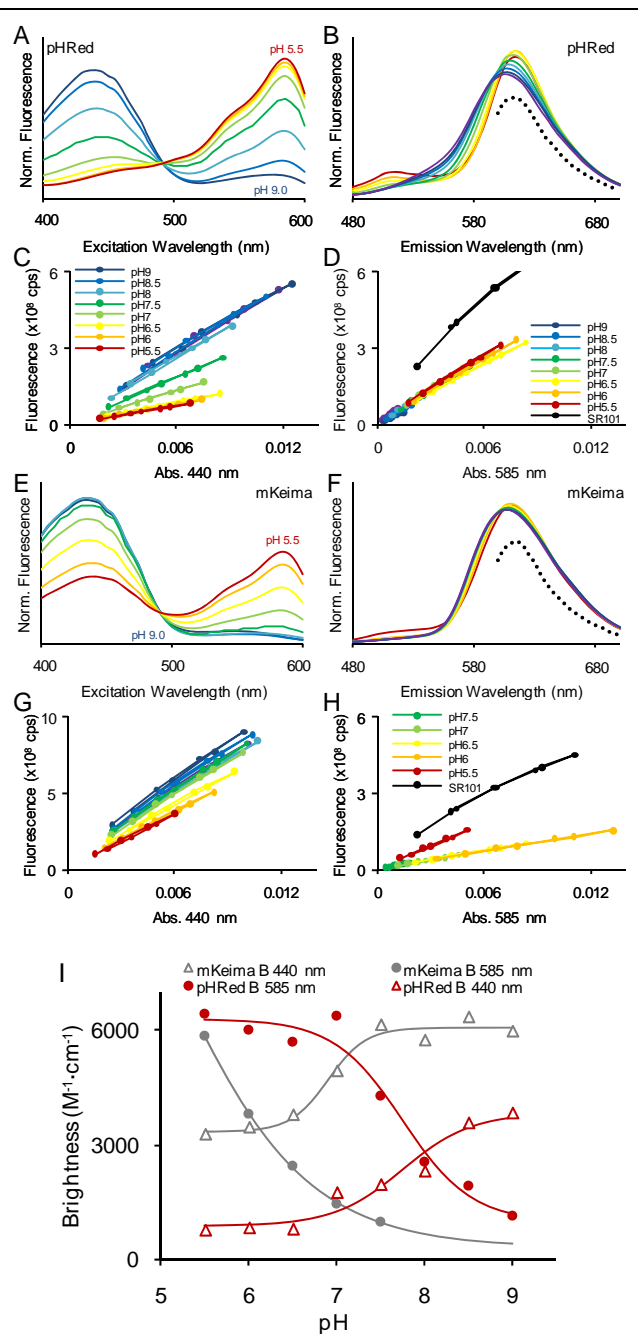
Photophysical properties of pHRed (Related to Figure 1a-e). Absorbance spectra were taken at 3-4 different protein concentrations at different pH to determine extinction coefficients (Supplemental Figure S2). At the end of each measurement, NaOH was added directly to the sample to a final concentration of 1M, and the 446 nm absorbance of the mature chromophore was measured.⁷ This provided a direct measurement of protein concentration to minimize errors due to pipetting.

Quantum yields were measured by comparing the slopes of the fluorescence versus absorbance relationships. 7 to 9 data points were collected for each slope determination (Supplemental Figure S3).

The extinction coefficients, quantum yields, and brightness products of pHRed and mKeima measured in this study are listed in Supplemental Table S1.



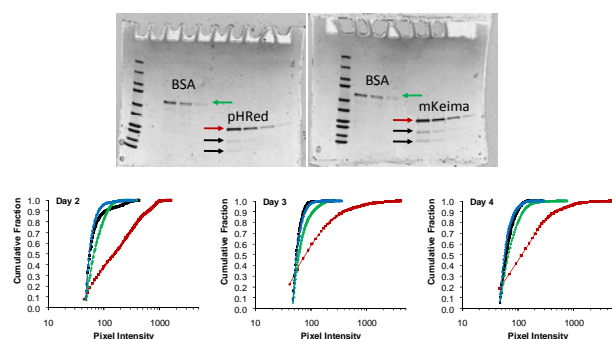
Supplemental Figure S2. pH dependence of the absorbance spectra of pHRed and mKeima. Extinction coefficients for absorbance at 440 and 585 nm were estimated by measuring absorbance spectra at 3 to 4 protein concentrations at pH 5.5 to pH 10.



Supplemental Figure S3. pH dependence of the fluorescence excitation and emission spectra of (a-b) pHRed and (e-f) mKeima. Quantum yields with excitation at 440 nm or 585 nm were determined by collecting fluorescence versus absorbance relationships, and comparing slopes to reference standards (mKeima, pH 7.5 for QY₄₄₀; Sulforhodamine 101 for QY₅₈₅). The brightness is the product of the quantum yield and extinction coefficient. (c-d) pHRed. (g-h) mKeima.

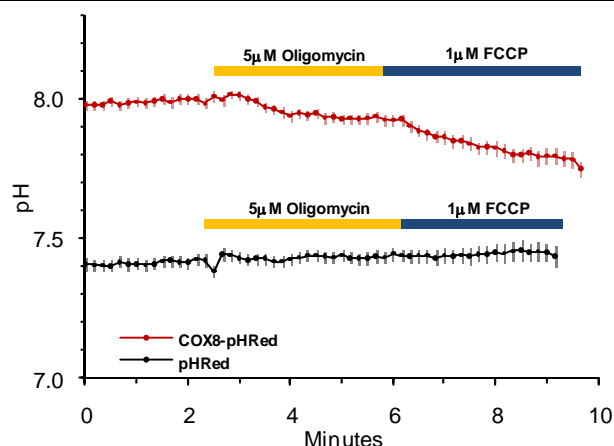
Purity of pHRed. Nickel affinity purified pHRed and mKeima were analyzed by denaturing SDS-PAGE. Densitometry of the Coomassie stained gels indicated the 26 kDa band accounted for ~90% of the protein. 10% of the protein was attributed to bands at ~16 kDa and ~10 kDa. These bands are previously described C- and N-terminal fragments that result from hydrolysis of the acylimine in the chromophore and backbone scission.² No other bands were apparent.

We also looked for any green fluorescence from pHRed. The fluorescence spectra of purified pHRed showed that there is no green fluorescent component. Because maturation can be different when FPs are expressed in mammalian cells, we also looked for green fluorescence following transfection of pHRed in N2A cells. Fluorescence images were taken 1, 2, 3, and 4 days after transfection (normally cells are used 3 and 4 days after transfection). On day 1 no fluorescence was visible. On days 2 to 4, we imaged 50 to 300 cells each day, exciting at 445 nm and collecting fluorescence images at 525 nm and 629 nm. We compared pixel intensities of transfected cells versus untransfected cells. We clearly observe an increase in red fluorescence, but there is not a significant green fluorescence component that would indicate a green immature population.



Supplemental Figure S4. Top: Densitometry following SDS-PAGE and Coomassie staining indicate both pHRed and mKeima were purified to at least 90% purity. Bottom: N2A cells were transfected with pHRed. Over time red fluorescence increased in transfected cells (red) versus autofluorescence from untransfected cells (black). There was not a significant green fluorescence in transfected cells (green) compared to autofluorescence of untransfected cells (blue).

pHRed Reported Dissipation of the Mitochondrial pH Gradient by FCCP (Related to Figure 3). COX8-pHRed reported acidification of the mitochondrial matrix induced by 1 μ M FCCP (Supplemental Figure S2, red trace, blue bar). This is consistent with the uncoupling action of FCCP which dissipates the mitochondrial inner membrane potential. Interestingly, oligomycin also caused a slight acidification which reached steady-state in ~1 min (yellow bar). This is contrary to the expected effect of oligomycin. Oligomycin would be expected to block the ATP synthase and proton translocation, causing an alkalization of the mitochondrial matrix. These contrary observations could be due to non-specific effects of oligomycin or indicative that ATP synthesis is not strongly coupled to the inner membrane potential in Neuro2A cells. However, exploration of this phenomenon is beyond the scope of this paper. Neither oligomycin nor FCCP significantly affected cytosolic pH as reported by pHRed (black trace).



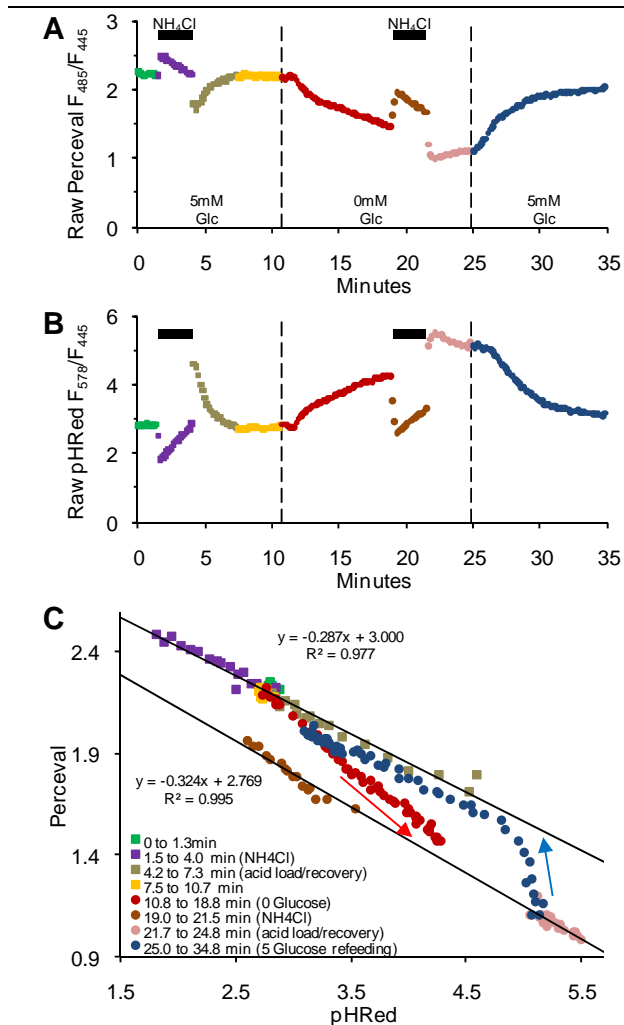
Supplemental Figure S5. pHRed expression in live Neuro2A reported on mitochondrial function. Expressed in the cytosol, pHRed indicated no change in intracellular pH in response to FCCP (blue bar). Targeted to the mitochondrial matrix, COX8-pHRed reported an acidification of the mitochondrial matrix with application of FCCP.

pH Correction of Perceval Using pHRed (Related to Figure 4).

The ATP:ADP ratio reporter Perceval is pH-sensitive. Thus, changes in the Perceval ratio shows significant changes that are correlated with the pHRed signal changes. To correct for pH artifacts, an empirical linear correlation was measured between Perceval and pHRed ratios during a change in intracellular pH that does not significantly affect the intracellular ATP:ADP ratio. For example, minor changes to the extracellular pH or mild alkalization by exposure to low concentrations of extracellular NH_4Cl are appropriate pH challenges. The linear correlation can be used in conjunction with the pHRed signal to extrapolate the expected changes in Perceval and thus normalize the Perceval ratio.

For example, Supplemental Figure S3 shows data from one cell extracted from Figure 4 of the main text. The uncorrected Perceval intensity ratio is strongly correlated to the pHRed intensity ratio, showing clear pH artifacts (Supplemental Figure S3ab). Using the NH_4Cl pulse in the presence of glucose when the intracellular ATP:ADP ratio is high and stable, data collected during this pH challenge show a strong linear correlation between Perceval and pHRed. Furthermore, data collected during the NH_4Cl pulse in the absence of glucose can be fitted with a near parallel line. These parallel fitted lines represent the extreme contours of the intracellular ATP:ADP ratio as reported by Perceval in its saturated and unsaturated states. Data points that are collinear along a contour have the same ATP:ADP ratio but differ in intracellular pH. When a time course of data points deviates between the two extreme contours, a real change in ATP:ADP occurred. In this experiment, extracellular glucose was withdrawn to deplete intracellular ATP. As a result, most points in the Perceval-pHRed space lie on the upper or lower fitted lines. Only when glucose was withdrawn did points (red) deviate from the top contour moving to the lower contour, indicating a real decrease in ATP:ADP. Likewise, when glucose was resupplied points (blue) deviated from the bottom contour and moved back towards the top contour, indicating a real increase in ATP:ADP.

Operationally, the linear correlation from individual cells is used to normalize Perceval and minimize pH artifacts. The predicted change in Perceval due to pH is calculated using the pHRed signal and fitted parameters, and then Perceval is normalized to the predicted pH-only change. As expected, this method is not a perfect correction for pH sensitivity. An alternative method is to use the estimated pH and pre-determined pH-dependence of Perceval reporting parameters to absolutely correct the Perceval signal. However, in practice this method suffers from large propagated errors and also relies on predetermined parameters. The empirical method works very well in practice (and in simple simulations), and has the added benefit of using parameters determined from each experiment on a cell-by-cell basis.



Supplemental Figure S6. Empirical correction of the pH-sensitivity of Perceval using pHRed from a live Neuro2A cell expressing both reporters. (A) Uncorrected Perceval ratio over time. 10 mM NH_4Cl pulses (black bars) were applied in the presence or absence of glucose. The fluorescence ratio trace is color coded to indicate time periods of interest throughout the figure. (B) pHRed ratio over time. (C) Data from (A) and (B) plotted as the Perceval ratio versus the pHRed ratio. Data during the NH_4Cl pulse in the presence of glucose provided a linear correlation between Perceval and pHRed (top solid black line). Data during the NH_4Cl pulse in the absence of glucose is fitted by a nearly parallel line (bottom black solid line) as expected. When glucose was withdrawn, the data points (red) deviate below the top fit, indicating a true decrease in intracellular ATP:ADP ratio (red arrow indicates progression over time). Conversely, when glucose was resupplied, the data points (blue) show a path from the lower fit to the upper fit, indicating a true increase in ATP:ADP ratio (blue arrow indicates progression over time). Cell “run down” at the end of the experiment can prevent complete recovery to the initial ATP:ADP ratio, causing the blue data points to lie close to but not on the top fitted line.

Supplemental Table S1. Photophysical properties of pHRed and mKeima measured in this study. Extinction coefficients were measured for the mature chromophore. Quantum yields for excitation at 440 nm and emission in the 550-700 nm band were measured against mKeima at pH 7.5, assumed to have a quantum yield of 0.24. Quantum yields for excitation at 585 nm and emission in the 600-700 nm band were measured against Sulforhodamine 101 in ethanol (QY = 0.95)¹¹ with correction for the difference in refractive indices. N.D. = Not determined.

pH	pHRed				mKeima			
	$\epsilon_{440 \text{ nm}}$	$\epsilon_{585 \text{ nm}}$	QY _{440 nm}	QY _{585 nm}	$\epsilon_{440 \text{ nm}}$	$\epsilon_{585 \text{ nm}}$	QY _{440 nm}	QY _{585 nm}
5.5	18000	15700	0.04	0.41	17700	13600	0.18	0.43
6.0	14200	14500	0.06	0.41	18500	13100	0.19	0.29
6.5	13800	13800	0.06	0.41	18600	7800	0.20	0.31
7.0	16500	14000	0.11	0.45	21200	4500	0.23	0.32
7.5	14800	8700	0.13	0.49	25600	2600	0.24	0.38
8.0	18300	6300	0.13	0.41	24900	1000	0.23	
8.5	22900	4000	0.16	0.48	25700	500	0.25	
9.0	21700	2540	0.18	0.44	22900	800	0.26	
pK _a	7.8	7.8	N.D.	N.D.	6.7	6.7	N.D.	N.D.

pH	pHRed		mKeima	
	($\epsilon \cdot \text{QY}$) ₄₄₀	($\epsilon \cdot \text{QY}$) ₅₈₅	($\epsilon \cdot \text{QY}$) ₄₄₀	($\epsilon \cdot \text{QY}$) ₅₈₅
5.5	800	6400	3300	5900
6.0	800	6000	3400	3800
6.5	800	5700	3800	2400
7.0	1700	6400	4900	1500
7.5	2000	4300	6100	1000
8.0	2300	2500	5700	
8.5	3600	1900	6400	
9.0	3800	1100	6000	
pK _a	7.8	7.8	6.9	N.D.

Supplemental References.

- (1) Kogure, T.; Karasawa, S.; Araki, T.; Saito, K.; Kinjo, M.; Miyawaki, A. *Nat. Biotechnol.* **2006**, *24*, 577-81.
- (2) Henderson, J. N.; Osborn, M. F.; Koon, N.; Gepshtein, R.; Huppert, D.; Remington, S. J. *J. Am. Chem. Soc.* **2009**, *131*, 13212-3.
- (3) Violot, S.; Carpentier, P.; Blanchoin, L.; Bourgeois, D. *J. Am. Chem. Soc.* **2009**, *131*, 10356-7.
- (4) Miesenbock, G.; De Angelis, D. A.; Rothman, J. E. *Nature* **1998**, *394*, 192-5.
- (5) Bizzarri, R.; Serresi, M.; Luin, S.; Beltram, F. *Anal. Bioanal. Chem.* **2009**, *393*, 1107-22.
- (6) Berg, J.; Hung, Y. P.; Yellen, G. *Nat. Methods* **2009**, *6*, 161-6.
- (7) Gross, L. A.; Baird, G. S.; Hoffman, R. C.; Baldrige, K. K.; Tsien, R. Y. *Proc. Natl. Acad. Sci. U.S.A.* **2000**, *97*, 11990-5.
- (8) Bulina, M. E.; Chudakov, D. M.; Mudrik, N. N.; Lukyanov, K. A. *BMC Biochem.* **2002**, *3*, 7.
- (9) Piatkevich, K. D.; Hult, J.; Subach, O. M.; Wu, B.; Abdulla, A.; Segall, J. E.; Verkhusha, V. V. *Proc. Natl. Acad. Sci. U.S.A.* **2010**, *107*, 5369-74.
- (10) Lin, M. Z.; McKeown, M. R.; Ng, H. L.; Aguilera, T. A.; Shaner, N. C.; Campbell, R. E.; Adams, S. R.; Gross, L. A.; Ma, W.; Alber, T.; Tsien, R. Y. *Chem Biol* **2009**, *16*, 1169-79.
- (11) Velapoldi, R. A.; Tonnesen, H. H. *J. Fluoresc.* **2004**, *14*, 465-72.